ROYAL SOCIETY OF CHEMISTRY

Check for updates

Effects of tuning decision trees in random forest regression on predicting porosity of a hydrocarbon reservoir. A case study: volve oil field, north sea

Kushan Sandunil, [iD] *[a] Ziad Bennour, [iD] [a] Hisham Ben Mahmud [iD] [b] and Ausama Giwelli [iD] [cd]

Machine learning (ML) has emerged as a powerful tool in petroleum engineering for automatically interpreting well logs and characterizing reservoir properties such as porosity. As a result, researchers are trying to enhance the performance of ML models further to widen their applicability in the real world. Random forest regression (RFR) is one such widely used ML technique that was developed by combining multiple decision trees. To improve its performance, one of its hyperparameters, the number of trees in the forest (*n_estimators*), is tuned during model optimization. However, the existing literature lacks in-depth studies on the influence of *n_estimators* on the RFR model when used for predicting porosity, given that *n_estimators* is one of the most influential hyperparameters that can be tuned to optimize the RFR algorithm. In this study, the effects of *n_estimators* on the RFR model in porosity prediction were investigated. Furthermore, *n_estimators*' interactions with two other key hyper-parameters, namely the number of features considered for the best split (*max_features*) and the minimum number of samples required to be at a leaf node (*min_samples_leaf*) were explored. The RFR models were developed using 4 input features, namely, resistivity log (RES), neutron porosity log (NPHI), gamma ray log (GR), and the corresponding depths obtained from the Volve oil field in the North Sea, and calculated porosity was used as the target data. The methodology consisted of 4 approaches. In the first approach, only *n_estimators* were changed; in the second approach, *n_estimators* were changed along with *max_features*; in the third approach, *n_estimators* were changed along with *min_samples_leaf*; and in the final approach, all three hyperparameters were tuned. Altogether 24 RFR models were developed, and models were evaluated using adjusted R^2 (adj. R^2), root mean squared error (RMSE), and their computational times. The obtained results showed that the highest performance with an adj. R^2 value of 0.8505 was achieved when *n_estimators* was 81, *max_features* was 2 and *min_samples_leaf* was 1. In approach 2, when *n_estimators*' upper limit was increased from 10 to 100, there was a test model performance growth of more than 1.60%, whereas increasing *n_estimators*' upper limit from 100 to 1000 showed a performance drop of around 0.4%. Models developed by tuning *n_estimators* from 1 to 100 in intervals of 10 had healthy test model adj. R^2 values and lower computational times, making them the best *n_estimators*' range and interval when both performances and computational times were taken into consideration to predict the porosity of the Volve oil field in the North Sea. Thus, it was concluded that by tuning only *n_estimators* and *max_features*, the performance of RFR models can be increased significantly.

[a] Curtin University Malaysia, 98009 Miri, Sarawak, Malaysia.
  E-mail: kwkushan@postgrad.curtin.edu.my
[b] Universiti Teknologi PETRONAS, 32610 Seri Iskandar, Perak Darul Ridzuan,
  Malaysia
[c] INPEX, 100 St Georges Terrace, 6000 Perth, WA, Australia
[d] WASM, Curtin University, Kensington, WA 6151, Australia

1. Introduction

Artificial intelligence (AI) has become a popular topic over the past few years due to its immense potential in STEM fields. Machine learning (ML) is a branch of AI where it learns with or without supervision to make predictions. Its abilities to predict or forecast outputs, decrease computational time, and extract features from complex and high-dimensional datasets make it a

great tool for working with complex and huge datasets.[1–3] The concept of ML was first put forward by Turing.[4] Since then, ML has seen a significant improvement with the invention of complex and high-performing algorithms. With the popularity of ML algorithms, like many other engineering sectors, their applicability in reservoir engineering has been tested, especially in porosity prediction. Porosity gives an idea about the fluid storage capacity, and it plays a vital role in the upstream oil and gas industry since it is used in estimating the petroleum initially in place in the reservoir. Core analysis is a reliable and widely accepted approach that is used to estimate porosity. However, this method is expensive and time-consuming. To address these challenges, petroleum engineers and researchers are investigating the applicability of ML in reservoir characterization. Random forest regression (RFR) is one such ML algorithm that has been successfully used to predict porosity. To enhance the performance of ML models, hyperparameter optimization is used. In this research, the effects of one of the main hyperparameters of RFR, the number of decision trees in the forest ($n\_estimators$) when predicting the porosity of a sandstone-dominated section in Volve oilfield have been investigated. Moreover, the behaviours of two other widely used hyperparameters in RFR, the minimum number of samples required to be at a leaf node ($min\_samples\_leaf$), and the number of features considered for the best split ($max\_features$) when tuned along with $n\_estimators$, have been studied. Apart from the primary objectives mentioned, this study tested the feasibility of an optimized RFR algorithm in reservoir characterization, specifically porosity prediction, and could be further extended to permeability and saturation predictions in future studies.

ML application in reservoir characterization has significantly increased over the last couple of decades due to its ability to tackle regression and classification-type problems.[5–7] With the evolution of ML, a notable number of algorithms have been introduced. The artificial neural network (ANN), which uses a parallel processing approach and was developed based on the function of a neuron of a human brain, has been utilized in petrophysical parameter prediction.[8,9] Support vector regression (SVR) is another algorithm developed in the initial stages of the ML timeline, and it can handle non-linear relationships between a set of inputs and an output. Moreover, SVR has been utilized widely in reservoir characterization.[10–13] The least absolute shrinkage and selection operator (LASSO) regression and Bayesian model averaging (BMA) have also been extensively used in ML-related studies in the literature.[14] BMA uses Bayes theorem and LASSO uses residual sums of squares to build a linear relationship between the inputs and the output. BMA and LASSO regressions have been used in permeability modelling in recent studies.[5] Apart from petrophysical parameter predictions, ML models have also been used in lithofacies classification.[15] Generally, these studies utilized ML approaches to model lithofacies sequences as a function of well-logging data to predict discrete lithofacies distribution at missing intervals.[16–18] Besides permeability prediction, water saturation estimation, and lithofacies classification, ML models have been used in reservoir porosity estimation, which is the parameter of focus in this study. ML
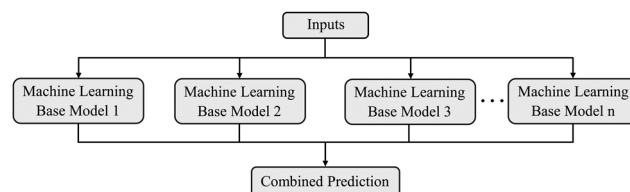

Fig. 1 Representation of the ensemble model.

algorithms, such as ANN, deep learning, and SVR, have been used to predict porosity using logging data, seismic attributes, and drilling parameters.[19–21]

Apart from the mentioned ML models, the ML approach known as ensemble learning has been applied in many recent studies. Here, ML base models (weaker models) are strategically combined to produce a high-performing and efficient model as shown in Fig. 1. Ensemble ML models have become a popular tool among researchers to predict petrophysical properties due to their ability to reduce overfitting and underfitting.[22–26] RFR is one such popular ensemble ML model that was developed by amalgamating multiple decision trees.[27]

Hyperparameter tuning is a process that is implemented to fine-tune ML algorithms to obtain optimal models.[28–30] Several hyperparameters can be controlled in an RFR model, such as $n\_estimators$, $max\_features$, $min\_samples\_leaf$, maximum depth of the tree (max_depth), fraction of the original dataset assigned to any individual tree ($max\_samples$), minimum number of samples required to split an internal node ($min\_samples\_split$), maximum leaf nodes to restrict the growth of the tree (max_leaf_nodes).

Hyperparameter optimization has been utilized in recent studies related to reservoir characterization. Wang et al. developed an RFR model to predict permeability in the Xishan Coalfield, China.[24] Five hyperparameters, $n\_estimators$, $max\_features$, max_depth, $min\_samples\_leaf$ and $min\_samples\_split$, were tuned during hyperparameter optimization. Zou et al. estimated reservoir porosity using a random forest algorithm.[31] During the hyperparameter optimization stage, $n\_estimators$, $max\_features$, $min\_samples\_leaf$, $min\_samples\_split$ and max_depth were tuned. Rezaee and Ekundayo tuned $n\_estimators$, $min\_samples\_leaf$, $min\_samples\_split$, and max_depth during the development of the RFR model used to predict the permeability of precipice sandstone in the Surat Basin, Australia.[32]

Even though hyperparameters have been tuned during the hyperparameter optimization phase of an ensemble ML model development, the literature lacks studies that specifically focus on the effects of hyperparameter tuning in ensemble learning when predicting petrophysical properties in reservoir characterization. Addressing this research gap, in this study, the authors investigated the influence of one of the most utilized hyperparameters in the literature, namely, the $n\_estimators$ of RFR, when predicting the porosity of a hydrocarbon reservoir. Also, the effects of $n\_estimators$ were studied along with another two widely used hyperparameters, $max\_features$ and $min\_samples\_leaf$, when predicting the porosity of the Volve oil field in the North Sea. The study considered a supervised learning

regression approach. The workflow of the study consisted of data preprocessing, RFR model development, and model analysis. Several RFR models were developed, including tuning *n_estimators*, tuning *n_estimators* along with *max_features*, tuning *n_estimators* along with *min_samples_leaf*, and tuning all three hyperparameters at once under four approaches by integrating grid search optimization and K-fold cross-validation. The models' performances were evaluated based on the adjusted coefficient of determination (adj. R^2), root mean squared error (RMSE), and computational time. Only the three aforementioned hyperparameters were considered due to processing capacity limitations; however, this study is expected to be a solid initiation towards the development of future studies on the effects of hyperparameters in ML algorithms in reservoir characterization.

2. Methodology

The development of an ML model involves multiple steps, namely, data acquisition, data preprocessing, model development, and data analysis.[33–35] In this study the abovementioned steps were implemented to develop robust ML models.

2.1 Geological setting and dataset

The Volve oil field (Fig. 2) was selected as the study area and the well log data of the field is publicly available. Several ML-related studies have been conducted using the Volve oil field datasets.[36–38] It was formed during the Jurassic period by the collapse of adjacent salt ridges. Oil was discovered in the field in 1993 in the middle Jurassic Hugin sandstone formations, identifying it as a clastic reservoir.

The Hugin Formation is 153 m thick and oil-bearing and was penetrated at 3796.5 m, approximately 60 m deeper than expected. The total oil column in the well was 80 m, but no clear oil–water contact was observed.[38,40] The reservoir section was made up of highly variable fine to coarse-grained, well to poorly-sorted subarkosic arenite sandstones with good to excellent reservoir properties. The Hugin Formation of the area consists of a shallow marine shoreface, coastal plain/lagoonal,

Fig. 2 Study area – Volve oil field's location in the North Sea. Adapted from Mapchart.[39]

channel, and possibly mouth bar deposits. The underlying Skagerrak Formation was completely tight due to extensive kaolinite and dolomite cementation. The current study used data from well 15/9-19A. The well was drilled through the Skagerrak Formation and terminated approximately 30 m into the Triassic Smith Bank Formation. To fully utilize the available data, the study considered data from the 3666.59 to 3907.08 m depth interval. This depth interval ran through three formations, namely, Draupne, Heather, and Hugin. The stratigraphic column and description of the vertical facies distribution of the section are shown in Fig. 3.

The dataset consisted of depth, well log data, and the corresponding calculated porosity values and had a total of 1547 data points. Three well log parameters, namely, resistivity log (RES), neutron porosity log (NPHI), and gamma-ray log (GR) along with corresponding depth were used as input features, and total porosity (PHIF) was used as the target data. PHIF was calculated using porosity from the density log (PHID) and NPHI. PHIF was derived from the density log, which was calibrated to overburden corrected core porosity for wells drilled with either oil-based mud or water-based mud. NPHI was used to correct for varying mud filtrate invasion. Eqn (1) and (2) were used to calculate PHIF and PHID, respectively.

$$\text{PHIF} = \text{PHID} + A \times (\text{NPHI} - \text{PHID}) + B \qquad (1)$$

$$\text{PHID} = \frac{\rho_{\text{ma}} - \rho_{\text{b}}}{\rho_{\text{ma}} - \rho_{\text{fl}}}. \qquad (2)$$

In eqn (1), A and B are regression coefficients and in eqn (2), ρ_{ma} is the matrix density, ρ_{b} is measured bulk density and ρ_{fl} is pore fluid density. Calculated PHIF values were assumed to be actual porosities during model development and evaluation.

2.2 Data preprocessing

The raw data acquired from the Volve oil field was subjected to data preprocessing before it was used in ML model development. Three main data preprocessing practices, namely, (i) data cleaning, (ii) feature scaling, and (iii) data division, were utilized in this study.[42–49] Under data cleaning, missing values and outliers were identified. Missing values were the sections where data points were missing from the dataset. Outliers include the data that were outside of a considered range in each feature. The interquartile range method was used to detect the outliers. Both missing data and outliers were treated by removing them completely from the dataset.[50,51]

Feature scaling is also a common practice implemented during data preprocessing. There are two widely used feature scaling approaches in the literature, namely, normalization and standardization. However, in this study feature scaling was neglected since RFR is a tree-based ML model where splits do not change with any monotonic transformation.[52]

Data division was carried out by splitting the dataset into 2 parts for training and testing. The training portion was used to train the ML models while the testing portion was used to test the trained models. The train-test ratio was considered as
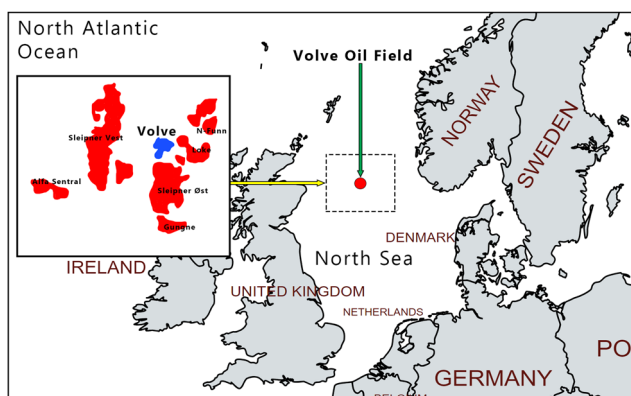
Stratigraphy				Depth (m)	Lithology	Lithological Description
System	Series	Group	Formation			
Jurassic	Upper Jurassic	Viking Group	Draupne Formation	3666.5		**Claystone:** Dark brown - brownish black, firm, blocky - subfissile, uniform, non-calcareous, carbonaceous
				3700		**Claystone:** Predominantly dark brown - brownish black - dusky yellowish brown, firm, blocky - subfissile, silty, non-calcareous, micromicaceous, carbonaceous
			Heather Formation	3706.0		**Claystone:** Olive black - grey black, firm, blocky, silty and sandy in parts **Limestone:** Medium grey - off white firm, blocky, silty and sandy in parts
				3750		**Claystone:** Olive black, firm - moderately hard, blocky silty, carbonaceous, micromicaceous, non-calcareous, rarely medium grey - dark green grey
				3796.5		**Claystone:** Medium dark grey - dark grey, occasionally green grey, firm **Limestone:** Medium dark grey - off white yellow brown, firm - moderate hard
		Vestland Group	Hugin Formation	3800		**Sandstone/Siltstone:** Light brown - off white matrix, clear - translucent quartz, silty - fine, trace medium, moderate -well sorted, subrounded to rounded, in parts grading to silty claystone, firm to friable, non calcareous **Siltstone:** Light to moderate brown, sandy -grading to very fine sandstone **Claystone:** Dark olive grey, medium brown, medium dark grey, firm, blocky, silty, in parts grading to siltstone
				3850		**Sandstone:** Brown grey, clear to translucent quartz, mainly fine - coarse, predominantly moderate - well sorted, friable - firm occasionally moderately carbonate cement and moderately hard, predominantly good visual porosity, mica lamina, carbonaceous/coal material and micropyrite is common in various amounts
				3900		**Sandstone:** Patches of coal, abundant micropyrites, else as above
				3908.0		**Dolomite:** Light grey brown, moderate hard, angular trace macrofossils, tight

Fig. 3 Stratigraphic column and facies description of the considered subsurface section. Adapted from Statoil.[41]

80:20, *i.e.*, 80% of the total dataset was allocated for training while the remaining 20% was used for testing.[53,54]

2.3 Machine learning model development

The RFR model is a combination of multiple decision trees. A typical architecture of an RFR model is shown in Fig. 4. Segal demonstrated the random forest algorithm mathematically as $h(x;\theta_r)$, $r = 1,\dots,R$, where x represents the observed input vector associated with the vector X.[55] X and θ_r are independent and identically distributed random vectors. For mathematical clarification we define a vector with numerical outcomes Y. Therefore, the training dataset of the RFR can be assumed to be drawn from a joint distribution of (X,Y).

For regression, the random forest prediction is the unweighted average over the collection:

$$h(x) = \left(\frac{1}{R}\right)\sum_{r=1}^{R} h(x;\theta_r). \tag{3}$$

As $r \to \infty$, the Law of Large Numbers ensures

$$E_{X,Y}(Y - \bar{h}(X))^2 \to E_{X,Y}(Y - E_\theta h(X;\theta))^2. \tag{4}$$
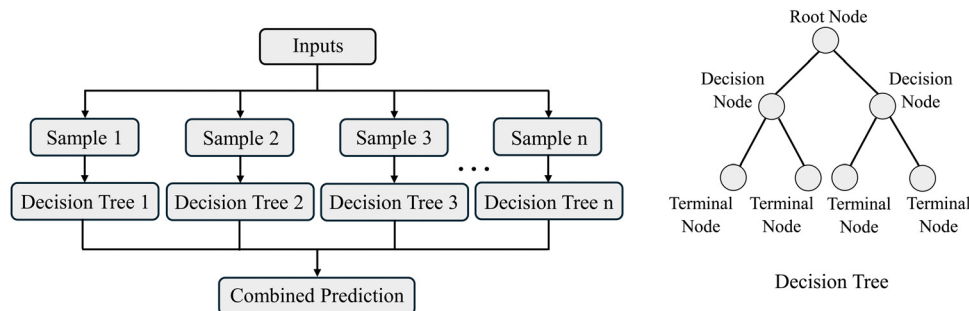
Fig. 4 Random Forest architecture (left) and the base model architecture (right).

The quantity on the right is the prediction (or generalization) error for the random forest, designated PE_f^*. The convergence in eqn (4) implies that random forests do not overfit.

Next, we define the average prediction error for an individual tree as $h(X;\theta)$

$$PE_f^* = E_\theta E_{X,Y}(Y - h(X;\theta))^2. \qquad (5)$$

Assuming that for all θ the tree is unbiased, *i.e.*, $EY = E_X h(X;\theta)$, then

$$PE_f^* \leq \bar{\rho} PE_f^* \qquad (6)$$

where $\bar{\rho}$ is the weighted correlation between residuals $Y - h(X;\theta)$ and $Y - h(X;\theta')$ for independent θ, θ'.

The inequality shown by eqn (6) highlights what is required for accurate RFR, which is having a low correlation between residuals of differing tree members of the forest and low prediction error for the individual trees. The model's performance can be further enhanced by tuning its hyperparameters.

During the study, RFR models were developed using the Python programming language. The cleaned dataset obtained during the data preprocessing stage was loaded into Python, then split into training and testing. The Python-based *scikit-learn* library's *RandomForestRegressor* was used to develop the RFR algorithm. The *RandomForestRegressor* comes with default hyperparameters built into it. Default values assigned to some of the main hyperparameters of RFR in *scikit-learn* are given in Table 1.

However, rather than using the default hyperparameters assigned by the *scikit-lean* library, to achieve the primary objectives of the study, hyperparameter optimization was implemented. Hyperparameter optimization is a commonly used practice to build robust ML models.[56,57] The hyperparameters of RFR

were tuned using the grid search optimization (GSO) approach. For this, the *GridSearchCV* optimization algorithm in the *scikit-learn* library was used. GSO was considered since it runs through all the possible combinations in the hyperparameter space, thus selecting the best combination of the space.[57,58] The hyperparameter space was predefined by including the possible values and it was fed into the GSO algorithm.

GSO was implemented along with random subsampling cross-validation. An approach known as the K-fold cross-validation was used. During the K-fold cross-validation, the training dataset is divided into K number of same-sized portions (folds), and K − 1 of the portions are used for training and the remainder are used for validation.[59,60] This is repeated until each fold gets the chance to be the validation set. For this study, a 5-fold cross-validation was implemented as shown in Fig. 5. Therefore, the training set was divided into five portions and during each split, four portions were used for training and one portion was used for validation.

Tuning was done under 4 approaches as shown in Fig. 6 to investigate the effects of the considered hyperparameters. In the first approach, *n_estimators* was changed from 1 to 10, 1 to 100, and 1 to 1000 in different intervals. The notation used to demonstrate the *n_estimators* change is shown in Table 2.

In the second approach, *n_estimators* was changed from 1 to 1000 in the same way as approach 1 along with *max_features*. Here, *max_features* was changed from 10% to 100% of total features in increments of 10%. In the third approach, *n_estimators* was changed in the same way along with *min_samples_leaf*. In this case, *min_samples_leaf* was changed from 1 to 20

Table 1 Some hyperparameters of the random forest algorithm and their default values in the *scikit-learn* library

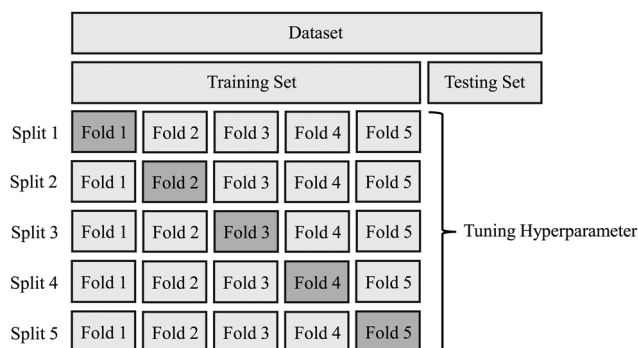| Hyperparameter	Default value
n_estimators	100
max_features	1.0
min_samples_leaf	1
max_depth	None
max_samples	None
min_samples_split	2
max_leaf_nodes	None

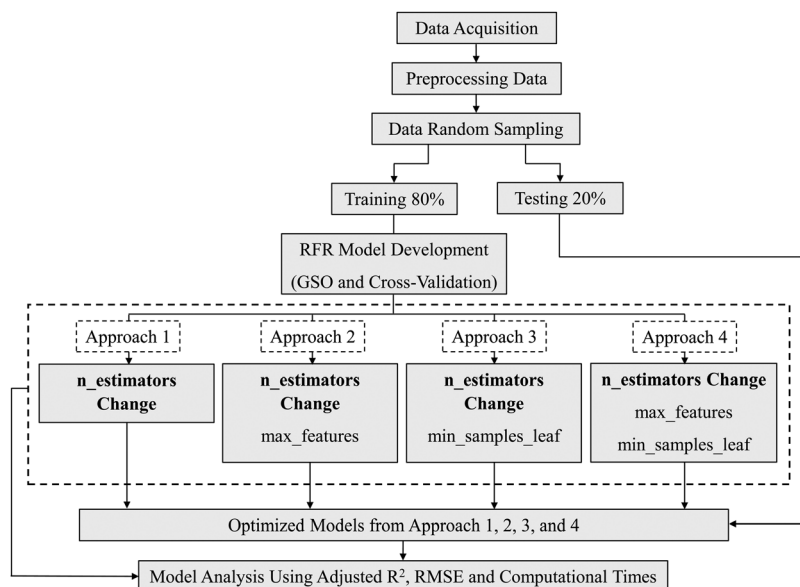**Fig. 5** Demonstration of the K-fold cross-validation.

Fig. 6 Workflow of the methodology.

Table 2 Notations of changes in *n_estimators* and their representations

n_estimators change notation	Starting value	Ending value	Increment
1:10:1	1	10	1
1:100:1	1	100	1
1:100:10	1	100	10
1:1000:1	1	1000	1
1:1000:10	1	1000	10
1:1000:100	1	1000	100

in intervals of 1. In the fourth approach, all 3 hyperparameters, *i.e.*, *n_estimators*, *max_features* and *min_samples_leaf* were varied at the same time in the above-mentioned intervals. In each approach, values of all the other hyperparameters of RFR were kept at their default values assigned by the *scikit-learn* library. The link to the GitHub folder with the developed codes is given in the appendix.

2.4 Results analysis

In the literature, the coefficient of determination (R^2) seems to be the go-to statistical parameter to evaluate the performance of the RFR models.[61–63] However, an improved version of R^2 known as the adjusted coefficient of determination (adj. R^2) was used in this study to evaluate the developed models since it takes the number of data points and the number of input features into consideration during evaluation.[5] The mathematical equation of R^2 is shown in eqn (7). Eqn (8) shows the mathematical equation of adj. R^2. The closer the adj. R^2 is to 1, the higher the performance of the model.

$$R^2 = 1 - \frac{\sum (y_i - \hat{y}_i)^2}{\sum (y_i - \bar{y}_i)^2}. \tag{7}$$

$$\mathrm{Adj}.R^2 = 1 - \frac{(1 - R^2)(n - 1)}{n - m - 1}. \tag{8}$$

In eqn (7) and (8), y_i is the actual value, $\hat{y}$ is the predicted value, $\bar{y}$ is the mean value of the distribution, n is the number of data points and m is the number of input features.

Apart from the adj. R^2, models were also evaluated using RMSE. The mathematical equation of RMSE is shown in eqn (9).

$$\mathrm{RMSE} = \sqrt{\frac{\sum (y_i - \hat{y}_i)^2}{n}}. \tag{9}$$

The developed RFR models were further evaluated based on their runtime to study how tuning considered hyperparameters affects computational times. The train–test difference was also used to further analyze the models. The train–test difference is an indication of the generalizability of an ML model, and it gives an idea about the variance of the model. The lower the train–test difference, the higher the generalizability of the model.[64,65]

3. Results and discussion

The adj. R^2 values obtained using approach 1 of the methodology are tabulated in Table 3. When only *n_estimators* increased from 1 to 10 in intervals of 1 (keeping all the other hyperparameters at their default values), the model yielded a training adj. R^2 of 0.9650, validation adj. R^2 of 0.8188 and testing adj. R^2 of 0.8024. The training score is higher than the validation (cross-validation) and testing scores as expected since the model is fitted (trained) to the training set and this pattern was observed in all the models developed during the study. In approach 1, when the upper limit of *n_estimators* value was increased from 10 to 100, the training, validation, and testing scores showed significant increases. The training score had an increase of 1.14%, the validation score had an increase of 2.19%, and the test score had an increase of 2.22%. This rise in performance

Table 3 Adjusted coefficients of determination, and computational times of the models obtained in approach 1

| Model no. | n_estimators change | n_estimators | Adj. R^2 | | | Computational time (s) |
			Training	Validation	Testing	
M11	1:10:1	8	0.9650	0.8188	0.8024	0.81
M12	1:100:1	51	0.9760	0.8367	0.8202	70.25
M13	1:100:10	51	0.9760	0.8367	0.8202	6.88
M14	1:1000:1	51	0.9760	0.8367	0.8202	6932.55
M15	1:1000:10	51	0.9760	0.8367	0.8202	707.56
M16	1:1000:100	801	0.9799	0.8352	0.8218	65.73
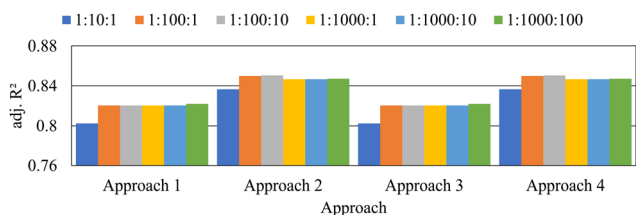
Fig. 7 Adjusted coefficient of determination values of each approach for different changes in n_estimators.

can be seen in Fig. 7 where the adj. R^2 values of the testing models were plotted for each approach.

Interestingly, when the upper limit of the n_estimators range was pushed beyond 100, the performance of the model did not show any noticeable increase in all training validation and testing adj. R^2 values. When n_estimators changed from 1 to 100 in intervals 1 and 10 (models M12 and M13) and n_estimators changed from 1 to 1000 in intervals 1 and 10 (models M14 and M15), the models showed the same performance, i.e. a training score of 0.9760, validation score of 0.8367 and a testing score of 0.8202. However, when the n_estimators changed from 1 to 1000 in intervals of 100, the training and testing scores of the M16 model showed a slight increase in performance, yielding an adj. R^2 of 0.9799 and 0.8218, respectively. However, the validation score showed a slight decrease, which was negligible.

The highest computational time of 6932.55 seconds was shown by the model M14 where n_estimators changed from 1 to 1000 in increments of 1. The results from approach 1 showed that after a certain n_estimators value, the models' performances increased drastically and the performance was maintained at a constant value over a certain n_estimators range showing that the performance of the RFR when n_estimators

was tuned was efficient within a certain range. Since the range and interval at which the n_estimators values are tuned affect the computational time, an effective range and an interval for n_estimators should be decided upon, taking computational time into account.

In approach 2, max_features were also tuned along with n_estimators. Results obtained using approach 2 of the methodology are tabulated in Table 4. As observed in approach 1, clear spikes in training, validation, and testing adj. R^2 values were observed when the upper limit of n_estimators was increased from 10 to 100. The training score had an increase of 1.36%, the validation score had an increase of 1.92%, and the test score had an increase of 1.60%. This clear jump in performance is noticeable in Fig. 7. Interestingly, the performances of the models developed in approach 2 were significantly higher than the performance of the corresponding "n_estimators change" in approach 1. This is quite visible in Fig. 8. Further, going from approach 1 to 2, the average validation score increased by 2.24% and the testing score increased by 3.52%, which was significant. This increase in adj. R^2 values is an indication that tuning max_features has a major impact on predicting the porosity using RFR. Model M21, where n_estimators were changed from 1 to 10 in intervals of 1 and max_features were changed from 0.1 to 1 in intervals of 0.1, showed the least performance with a training score of 0.9672, validation score of 0.8381, and a testing score of 0.8366. On the other hand, model M23 showed the highest testing performance with an adj. R^2 of 0.8505 where n_estimators changed from 1 to 100 in intervals of 10 and max_features changed from 0.1 to 1 in intervals of 0.1. The model M23 yielded its best test model when n_estimators was 81 and max_features were 0.5. It should be noted that even though model M23 had the highest testing score, the training, and validation scores were not the best out of all the models

Table 4 Adjusted coefficients of determination, and computational times of the models obtained in approach 2

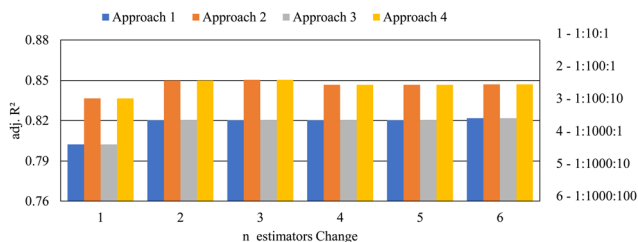| Model no. | n_estimators change | n_estimators | max_features | Adj. R^2 | | | Computational time (s) |
				Training	Validation	Testing	
M21	1:10:1	9	0.1	0.9672	0.8381	0.8366	3.69
M22	1:100:1	79	0.5	0.9804	0.8542	0.8500	326.56
M23	1:100:10	81	0.5	0.9806	0.8541	0.8505	30.20
M24	1:1000:1	520	0.5	0.9823	0.8556	0.8467	32 620.39
M25	1:1000:10	521	0.5	0.9823	0.8556	0.8467	3045.27
M26	1:1000:100	801	0.5	0.9823	0.8554	0.8471	284.29

Fig. 8 Adjusted coefficient of determination values for each change in $n\_estimators$ for different approaches.

developed in approach 2. The highest training score of 0.9823 was shown by models M24, M25, and M26. The highest validation scores were shown by models M24 and M25. However, it is more meaningful to select model M23 as the best-performing model since the testing set represents an independent dataset that had never been seen by the model before.

The anomaly in the validation score observed when the $n\_estimators$ were changed from 1 to 1000 in intervals of 100 in approach 1 was also observable in approach 2. The difference in train–test scores provides an idea about the generalizability of the model. The smaller the train–test difference, the higher the generalizability of the model. Overall, the train–test difference in approach 2 was noticeably less than that of approach 1. The average train–test difference decreased by 15.51% on going from approach 1 to 2. This showed that the generalizability of the models improved when $max\_features$ was introduced into the hyperparameter space. Similar to approach 1, the highest runtime was shown when the $n\_estimators$ changed from 1 to 1000 in increments of 1.

In approach 3, $n\_estimators$ was investigated with the alteration of $min\_samples\_leaf$, and the results obtained are tabulated in Table 5. Notably, all the performance results obtained for all

the RFR models except the runtimes were the same as that of approach 1, as seen in Fig. 7 and 8. This was because the optimum value selected by the grid search optimization of the $min\_samples\_leaf$ was the same as the default value assigned by the *scikit-learn* library for the RFR algorithm, hence the best testing adj. R^2 was shown by model M34 when the $n\_estimators$ was changed from 1 to 1000 in intervals of 100. Computational times were longer than those obtained in approach 1 since models developed in approach 3 had a larger hyperparameter space as compared to approach 1.

In approach 4, $n\_estimators$ was changed along with both $max\_features$ and $min\_samples\_leaf$. The results in Table 6 show that the performances of the models were the same as that of approach 2. A similar phenomenon caused this performance similarity as observed between approach 1 and approach 3. In this case, the default value for $min\_samples\_leaf$ was always selected during the tuning process and the $max\_features$ selected for the optimum model was similar to that of approach 2. Approach 4 had the longest computational time since 3 hyperparameters had to be tuned simultaneously. The highest runtime for all models was recorded in this approach by model M44, which was 82 832.02 seconds. In approach 4, as also observed in approach 2, there was a test model performance increase of 1.60% when the upper limit of $n\_estimators$ was increased from 10 to 100. When the upper limit was increased from 100 to 1000, there was a test model performance drop of around 0.4%.

Table 7 shows the RMSE values of approaches 1, 2, 3, and 4. While the adj. R^2 values give an idea about the correlation between the actual porosities and the predicted porosities, the RMSE values provide an idea about the difference (or the error) between the two. Therefore, RMSE is also an important parameter in ML model performance evaluation. The pattern in which RMSE values fluctuated in the 4 approaches was similar

Table 5 Adjusted coefficients of determination, and computational times of the models obtained in approach 3

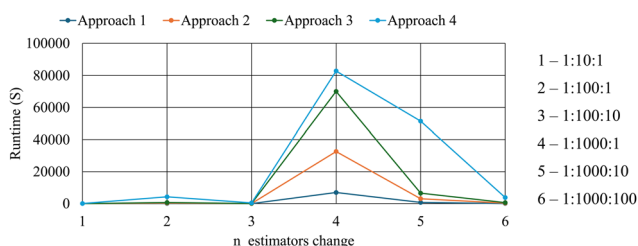| Model no. | $n\_estimators$ change | $n\_estimators$ | $min\_samples\_leaf$ | Adj. R^2 | | | Computational time (s) |
				Training	Validation	Testing	
M31	1:10:1	8	1	0.9650	0.8188	0.8024	7.79
M32	1:100:1	51	1	0.9760	0.8367	0.8202	674.81
M33	1:100:10	51	1	0.9760	0.8367	0.8202	64.96
M34	1:1000:1	51	1	0.9760	0.8367	0.8202	70 039.55
M35	1:1000:10	51	1	0.9760	0.8367	0.8202	6525.18
M36	1:1000:100	801	1	0.9799	0.8352	0.8218	606.28

Table 6 Adjusted coefficients of determination, and computational times of the models obtained in approach 4

| Model no. | $n\_estimators$ change | $n\_estimators$ | $max\_features$ | $min\_samples\_leaf$ | Adj. R^2 | | | Computational time (s) |
					Training	Validation	Testing	
M41	1:10:1	9	0.1	1	0.9672	0.8381	0.8366	56.22
M42	1:100:1	79	0.5	1	0.9804	0.8542	0.8500	4242.86
M43	1:100:10	81	0.5	1	0.9806	0.8541	0.8505	425.65
M44	1:1000:1	520	0.5	1	0.9823	0.8556	0.8467	82 832.02
M45	1:1000:10	521	0.5	1	0.9823	0.8556	0.8467	51 444.27
M46	1:1000:100	801	0.5	1	0.9823	0.8554	0.8471	3796.99

Table 7 RMSE of training and testing models of approaches 1, 2, 3, and 4

				RMSE						
Approach 1			Approach 2			Approach 3			Approach 4		
Model no.	Training	Testing	Model no.	Training	Testing	Model no.	Training	Testing	Model no.	Training	Testing
M11	1.2894	2.9967	M21	1.2516	2.7218	M31	1.2894	2.9967	M41	1.2516	2.7218
M12	1.0817	2.8499	M22	0.9835	2.5917	M32	1.0817	2.8499	M42	0.9835	2.5917
M13	1.0817	2.8499	M23	0.9798	2.5875	M33	1.0817	2.8499	M43	0.9798	2.5880
M14	1.0817	2.8499	M24	0.9399	2.6190	M34	1.0817	2.8499	M44	0.9399	2.6190
M15	1.0817	2.8499	M25	0.9396	2.6187	M35	1.0817	2.8499	M45	0.9396	2.6187
M16	0.9988	2.8312	M26	0.9396	2.6148	M36	0.9988	2.8312	M46	0.9396	2.6148

Fig. 9 Runtimes of the models of each $n\_estimators$' change for different approaches.

to that of adj. R^2. The smallest RMSEs were shown by model M16 with a training model RMSE of 0.9988 and a testing model RMSE of 2.8312. The improvement in the results when $max\_features$ was introduced into the hyperparameter space was also

evident based on the RMSE values obtained in approach 2. There was a clear decrease in RMSE values in both training and testing models in approaches 2 and 4 where $max\_features$ was tuned.

Runtime and grid search combinations had a positive relationship, $i.e.$, when the number of combinations in the grid search space was the largest, the runtime of the model was the highest, and $vice\ versa$. Further, it was observed that from approach 1 to approach 3, the increase in computational times was roughly proportional to each other as seen in Fig. 9. However, in approach 4 where $n\_estimators$ was changed along with the tuning of $max\_features$ and $min\_samples\_leaf$, an anomaly was observed when $n\_estimators$ was changed from 1 to 1000 in intervals of 10.

Even though the primary objective of the study was to investigate the influences of $n\_estimators$ along with $max\_features$ and $min\_samples\_leaf$ on the performance of RFR,
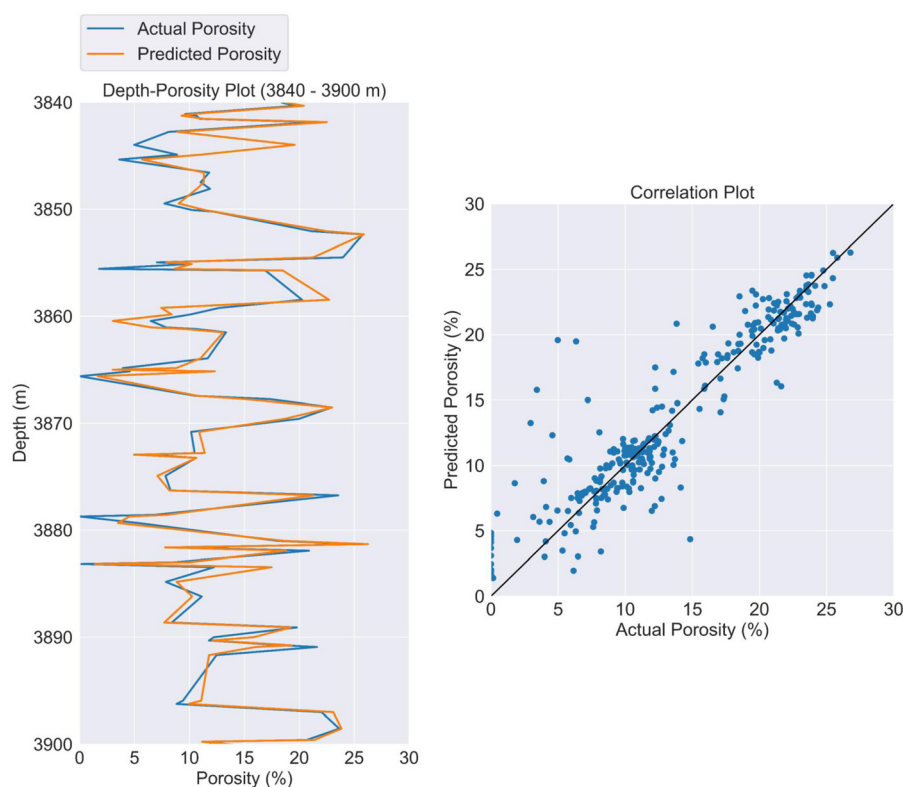

Fig. 10 Depth-porosity and correlation plots obtained from the predictions of the best-performing RFR testing model.

having an overall picture of the variation of the actual and predicted porosity and their relationship is important to understand the model's applicability in porosity prediction. To achieve this, depth-porosity graphs and correlation plots were plotted. Fig. 10 shows one such depth-porosity graph and a correlation plot developed for the best-performing RFR test model (model M23) of the study. The depth-porosity plot indicated that most of the time, the predicted porosity followed the pattern of the actual porosity. The correlation plot showed that the majority of the points were scattered around the perfect correlation line, which is an indication of a high correlation between the actual values and the predicted values.

4. Conclusions

The aim of this study was to examine the effects of tuning the number of decision trees in the forest (*n_estimators*) in random forest regression (RFR) for predicting porosity within the Volve oil field in the North Sea. Additionally, the study investigated the influence of *n_estimators* when tuned with two other commonly used hyperparameters, namely, the number of features to consider when looking for the best split (*max_features*) and the minimum number of samples required to be at a leaf node (*min_samples_leaf*). The hyperparameters were tuned using grid search optimization integrating 5-fold cross-validation, and model performances were evaluated based on adj. R^2, RMSE, and computational times.

• Overall, based on both the performance and computational time, the RFR model with *n_estimators* at 81 and *max_features* at 2 (while keeping all the other hyperparameters at their default values), which was developed in approach 2, produced the most effective model for predicting the porosity of the Volve oil field in the North Sea with a testing model adj. R^2 of 0.8505, a testing model RMSE of 2.5875, and a computational time of 30.2 seconds.

• There was a notable increase in performance when the upper limit of the *n_estimators* increased from 10 to 100. On the other hand, the performance of the models did not increase significantly when the upper limit of *n_estimators* increased from 100 to 1000. This phenomenon indicated that identifying an effective *n_estimators* range that is not too low (which will make the performance significantly low) and not too high (which will increase the computational time) is important to produce an efficient RFR model during porosity prediction.

• A range of 1 to 100 changed in intervals of 10 can be suggested for *n_estimators* when developing an RFR model to predict the porosity of the Volve oil field since these models showed higher performances and lower computational times in all four approaches. When the *n_estimators* range of 1 to 100 was changed in intervals of 10, it always yielded a high adj. R^2 value (in approaches 2 and 4, it yielded the highest testing model adj. R^2 value) for the model and had the second least computational time.

• When *n_estimators* was tuned along with *max_features* in approach 2, the results improved drastically as compared to approach 1 where only *n_estimators* was tuned. There was an average validation score increase of 2.24% and a testing score increase of 3.52% on going from approach 1 to 2. This improvement of the scores (adj. R^2) showed that *max_features* has a significant influence on the RFR model's performance.

• It was observed that computational time was largely affected by the number of hyperparameters altered, their range, and interval. Of all the approaches, the longest computational time was when *n_estimators* was tuned from 1 to 1000 in intervals of 1 along with *max_features* and *min_samples_leaf*.

Based on the results, only by adjusting *n_estimators* and *max_features* can an RFR model be developed with a robust prediction power to estimate the porosity in the Volve oil field.

Recommendations

This study focused on three hyperparameters, namely, *n_estimators*, *max_features* and *min_samples_leaf*. Apart from these hyperparameters, *min_samples_split* and *max_depth* are also widely used in the literature during hyperparameter optimization in RFR. Therefore, for future studies, it is recommended that the behaviour of *min_samples_split* and *max_depth* along with *n_estimators* be investigated.

Abbreviation

AI	Artificial intelligence
ML	Machine learning
RFR	Random forest regression
ANN	Artificial neural network
SVR	Support vector regression
LASSO	Least absolute shrinkage and selection operator
BMA	Bayesian model averaging
GSO	Grid search optimization
RMSE	Root mean squared error
R^2	Coefficient of determination
adj. R^2	Adjusted coefficient of determination
RES	Resistivity log
NPHI	Neutron porosity log
GR	Gamma ray log
PHIF	Total porosity
PHID	Porosity from density log
n_estimators	Number of trees in the forest
max_features	Number of features considered for the best split
min_samples_leaf	Minimum number of samples required to be at a leaf node
max_depth	Maximum depth of the tree
max_samples	Fraction of the original dataset assigned to any individual tree
min_samples_split	Minimum number of samples required to split an internal node
max_leaf_nodes	Maximum leaf nodes to restrict the growth of the tree
A	A regression coefficient

B	A regression coefficient
ρ_{ma}	Matrix density
ρ_b	Measured bulk density
ρ_{fl}	Pore fluid density
n	Number of datapoints
m	Number of input features
X	Independent and identically distributed random vector
θ_r	Independent and identically distributed random vector
x	Observed input vector associated with vector X
Y	A vector with numerical outcomes
y_i	Actual value
$\hat{y}$	Predicted value
$\bar{y}$	Mean value of the distribution

Author contributions

Kushan Sandunil: conceptualization, data curation, formal analysis, investigation, methodology, validation, visualization, writing – original draft. Ziad Bennour: conceptualization, methodology, supervision, funding acquisition, resources, writing – review & editing. Hisham Ben Mahmud: supervision, funding acquisition, writing – review & editing. Ausama Giwelli: supervision, writing – review & editing.

Data availability

Data for this article, including codes and graphs are available at GitHub at **https://github.com/kwkushan/effects-of-tuning-decision-trees-in-random-forest-regression-on-predicting-porosity-kushan-sandunil-**. A description about the available files in GitHub repository can be found in the appendix.

Conflicts of interest

The authors declare that they have no known competing financial interests or personal relationships that could have appeared to influence the work reported in this paper.

Appendix

The authors would like to share open repository folder containing the codes and resources for this study on **GitHub** and extend an invitation to collaborate through Open Knowledge sharing. In the folder, 4 codes are provided; Code_1 was developed by only tuning *n_estimators*. Code_2 was developed by tuning *n_estimators* along with *max_features*. Code_3 was developed by tuning *n_estimators* along with *min_samples_leaf* and the Code_4 was developed by tuning all three hyperparameters, *i.e.*, *n_estimators*, *max_features* and *min_samples_leaf*. The GitHub repository with the developed codes in the study

can be accessed *via* this **https://github.com/kwkushan/effects-of-tuning-decision-trees-in-random-forest-regression-on-predicting-porosity-kushan-sandunil-**.

References

1 C. Kavuri and S. L. Kokjohn, Exploring the potential of machine learning in reducing the computational time/expense and improving the reliability of engine optimization studies, *Int. J. Engine Res.*, 2020, **21**(7), 1251–1270.

2 N. Zhan and J. R. Kitchin, Uncertainty quantification in machine learning and nonlinear least squares regression models, *AIChE J.*, 2022, **68**(6), e17516.

3 X. Zhang, Y. Tian, L. Chen, X. Hu and Z. Zhou, Machine learning: a new paradigm in computational electrocatalysis, *J. Phys. Chem. Lett.*, 2022, **13**(34), 7920–7930.

4 A. M. Turing, *Computing machinery and intelligence*, Springer, Netherlands, 2009.

5 W. J. Al-Mudhafar, Bayesian and LASSO regressions for comparative permeability modeling of sandstone reservoirs, *Nat. Resour. Res.*, 2019, **28**(1), 47–62.

6 C. Ojukwu, K. Smith, N. Kadkhodayan, M. Leung and K. Baldwin, Reservoir Characterization, Machine Learning and Big Data–An Offshore California Case Study. InSPE Nigeria Annual International Conference and Exhibition 2020 Aug 11 (p. D013S002R005). SPE.

7 A. A. Silva, M. W. Tavares, A. Carrasquilla, R. Misságia and M. Ceia, Petrofacies classification using machine learning algorithms, *Geophysics.*, 2020, **85**(4), WA101–WA113.

8 M. Amiri, J. Ghiasi-Freez, B. Golkar and A. Hatampour, Improving water saturation estimation in a tight shaly sandstone reservoir using artificial neural network optimized by imperialist competitive algorithm–A case study, *J. Pet. Sci. Eng.*, 2015, **127**, 347–358.

9 S. Elkatatny, M. Mahmoud, Z. Tariq and A. Abdulraheem, New insights into the prediction of heterogeneous carbonate reservoir permeability from well logs using artificial intelligence network, *Neural Comput. Appl.*, 2018, **30**, 2673–2683.

10 K. O. Akande, T. O. Owolabi, S. O. Olatunji and A. AbdulRaheem, A hybrid particle swarm optimization and support vector regression model for modelling permeability prediction of hydrocarbon reservoir, *J. Pet. Sci. Eng.*, 2017, **150**, 43–53.

11 S. Baziar, H. B. Shahripour, M. Tadayoni and M. Nabi-Bidhendi, Prediction of water saturation in a tight gas sand-stone reservoir by using four intelligent methods: a comparative study, *Neural Comput. Appl.*, 2018, **30**, 1171–1185.

12 F. Anifowose, A. Abdulraheem and A. Al-Shuhail, A parametric study of machine learning techniques in petroleum reservoir permeability prediction by integrating seismic attributes and wireline data, *J. Pet. Sci. Eng.*, 2019, **176**, 762–774.

13 M. Z. Kamali, S. Davoodi, H. Ghorbani, D. A. Wood, N. Mohamadian, S. Lajmorak, V. S. Rukavishnikov, F. Taherizade and S. S. Band, Permeability prediction of heterogeneous carbonate gas condensate reservoirs applying group method of data handling, *Mar. Pet. Geol.*, 2022, **139**, 105597.

14 W. Al-Mudhafar Integrating bayesian model averaging for uncertainty reduction in permeability modeling. Inoffshore technology conference 2015 May 4 (pp. OTC-25646). OTC.

15 G. Wang, Y. Ju, C. Li, T. R. Carr and G. Cheng Application of artificial intelligence on black shale lithofacies prediction in Marcellus Shale, Appalachian Basin. InUnconventional Resources Technology Conference, Denver, Colorado, 25-27 August 2014 2014 Aug 27 (pp. 1970–1980). Society of Exploration Geophysicists, American Association of Petroleum Geologists, Society of Petroleum Engineers.

16 W. J. Al-Mudhafar, Integrating well log interpretations for lithofacies classification and permeability modeling through advanced machine learning algorithms, *J. Pet. Explor. Prod. Technol.*, 2017, **7**(4), 1023–1033.

17 W. J. Al-Mudhafar, Integrating lithofacies and well logging data into smooth generalized additive model for improved permeability estimation: Zubair formation, South Rumaila oil field, *Mar. Geophys. Res.*, 2019, **40**, 315–332.

18 J. Kim, Lithofacies classification integrating conventional approaches and machine learning technique, *J. Nat. Gas Sci. Eng.*, 2022, **100**, 104500.

19 S. R. Na'imi, S. R. Shadizadeh, M. A. Riahi and M. Mirzakhanian, Estimation of reservoir porosity and water saturation based on seismic attributes using support vector regression approach, *J. Appl. Geophys.*, 2014, **107**, 93–101.

20 A. Al-AbdulJabbar, K. Al-Azani and S. Elkatatny, Estimation of reservoir porosity from drilling parameters using artificial neural networks, *Petrophysics*, 2020, **61**(03), 318–330.

21 W. Chen, L. Yang, B. Zha, M. Zhang and Y. Chen, Deep learning reservoir porosity prediction based on multilayer long short-term memory network, *Geophysics*, 2020, **85**(4), WA213–WA225.

22 F. A. Anifowose Ensemble machine learning: the latest development in computational intelligence for petroleum reservoir characterization. InSPE Kingdom of Saudi Arabia Annual Technical Symposium and Exhibition 2013 May 19 (pp. SPE-168111). SPE.

23 A. Subasi, M. F. El-Amin, T. Darwich and M. Dossary, Permeability prediction of petroleum reservoirs using stochastic gradient boosting regression, *J. Ambient Intell. Humaniz. Comput.*, 2022, 1.

24 J. Wang, W. Yan, Z. Wan, Y. Wang, J. Lv and A. Zhou, Prediction of permeability using random forest and genetic algorithm model, *Comput. Model. Eng. Sci.*, 2020, **125**(3), 1135–1157.

25 D. A. Otchere, T. O. Ganat, R. Gholami and M. Lawal, A novel custom ensemble learning model for an improved reservoir permeability and water saturation prediction, *J. Nat. Gas Sci. Eng.*, 2021, **91**, 103962.

26 Z. Zhang and Z. Cai, Permeability prediction of carbonate rocks based on digital image analysis and rock typing using random forest algorithm, *Energy Fuels*, 2021, **35**(14), 11271–11284.

27 T. H. Lee, A. Ullah and R. Wang, Bootstrap aggregating and random forest, *Macroeconomic forecasting in the era of big data: Theory and practice*, 2020, pp. 389–429.

28 M. M. Maher and S. Sakr Smartml: A meta learning-based framework for automated selection and hyperparameter tuning for machine learning algorithms. InEDBT: 22nd International conference on extending database technology 2019 Mar 26.

29 L. Yang and A. Shami, On hyperparameter optimization of machine learning algorithms: Theory and practice, *Neurocomputing*, 2020, **415**, 295–316.

30 J. Isabona, A. L. Imoize and Y. Kim, Machine learning-based boosted regression ensemble combined with hyperparameter tuning for optimal adaptive learning, *Sensors*, 2022, **22**(10), 3776.

31 C. Zou, L. Zhao, M. Xu, Y. Chen and J. Geng, Porosity prediction with uncertainty quantification from multiple seismic attributes using random forest, *J. Geophys. Res.: Solid Earth*, 2021, **126**(7), e2021JB021826.

32 R. Rezaee and J. Ekundayo, Permeability prediction using machine learning methods for the CO_2 injectivity of the precipice sandstone in Surat Basin, Australia, *Energies*, 2022, **15**(6), 2053.

33 S. García, J. Luengo and F. Herrera, Introduction to data preprocessing, in *Data preprocessing in data mining*, ed. J. Kacprzyk and L. C. Jain, Springer International Publishing, Cham, Switzerland, 2015, pp. 10–13.

34 V. Gudivada, A. Apon and J. Ding, Data quality considerations for big data and machine learning: Going beyond data cleaning and transformations, *Int. J. Adv. Softw.*, 2017, **10**(1), 1–20.

35 K. Maharana, S. Mondal and B. Nemade, A review: Data pre-processing and data augmentation techniques, *Global Transit. Proceedings*, 2022, **3**(1), 91–99.

36 A. Al Ghaithi and M. Prasad Machine learning with artificial neural networks for shear log predictions in the Volve field Norwegian North Sea. InSEG Technical Program Expanded Abstracts 2020 2020 Sep 30 (pp. 450–454). Society of Exploration Geophysicists.

37 C. S. Ng, A. J. Ghahfarokhi and M. N. Amar, Well production forecast in Volve field: Application of rigorous machine learning techniques and metaheuristic algorithm, *J. Pet. Sci. Eng.*, 2022, **208**, 109468.

38 N. O. Nikitin, I. Revin, A. Hvatov, P. Vychuzhanin and A. V. Kalyuzhnaya, Hybrid and automated machine learning

approaches for oil fields development: The case study of Volve field, North Sea, *Comput. Geosci.*, 2022, **161**, 105061.

39 Mapchart. World map: simple [Internet]. 2024 [cited 2024 Jul 22]. Available from: **https://www.mapchart.net/world.html**.

40 S. Sen and S. S. Ganguli Estimation of pore pressure and fracture gradient in Volve field, Norwegian North Sea. InSPE Oil and Gas India Conference and Exhibition. 2019 Apr 8 (p. D022S027R002). SPE.

41 Statoil. 15/9-19A Well Composite Log, Sleipner, Theta Vest Prospect Structure [Internet]. 1998 [cited 2023 Mar 1]. Available from: **https://discovervolve.com/citation-non-commerciality-clause/**.

42 I. F. Ilyas and X. Chu, *Data cleaning*, Morgan & Claypool, 2019.

43 A. Jain, H. Patel, L. Nagalapatti, N. Gupta, S. Mehta, S. Guttula, S. Mujumdar, S. Afzal, R. Sharma Mittal and V. Munigala Overview and importance of data quality for machine learning tasks. InProceedings of the 26th ACM SIGKDD international conference on knowledge discovery & data mining 2020 Aug 23 (pp. 3561–3562).

44 S. Rawat, A. Rawat, D. Kumar and A. S. Sabitha, Application of machine learning and data visualization techniques for decision support in the insurance sector, *Int. J. Inf. Manag. Data Insights*, 2021, **1**(2), 100012.

45 M. M. Ahamad, S. Aktar, M. Rashed-Al-Mahfuz, S. Uddin, P. Liò, H. Xu, M. A. Summers, J. M. Quinn and M. A. Moni, A machine learning model to identify early stage symptoms of SARS-Cov-2 infected patients, *Expert Syst. Appl.*, 2020, **160**, 113661.

46 I. H. Sarker, Y. B. Abushark, F. Alsolami and A. I. Khan, Intrudtree: a machine learning based cyber security intrusion detection model, *Symmetry*, 2020, **12**(5), 754.

47 H. Feizi, H. Apaydin, M. T. Sattari, M. S. Colak and M. Sibtain, Improving reservoir inflow prediction via rolling window and deep learning-based multi-model approach: case study from Ermenek Dam, Turkey, *Stoch. Environ. Res. Risk Assess.*, 2022, **36**(10), 3149–3169.

48 J. J. Salazar, L. Garland, J. Ochoa and M. J. Pyrcz, Fair train-test split in machine learning: Mitigating spatial autocorrelation for improved prediction accuracy, *J. Pet. Sci. Eng.*, 2022, **209**, 109885.

49 G. M. Mask and X. Wu Deriving New Type Curves through Machine Learning in the Wolfcamp Formation. InSPE Reservoir Characterisation and Simulation Conference and Exhibition. 2023 Jan 24 (p. D011S001R007). SPE.

50 T. Emmanuel, T. Maupong, D. Mpoeleng, T. Semong, B. Mphago and O. Tabona, A survey on missing data in machine learning, *J. Big Data*, 2021, **8**, 1–37.

51 M. M. Seliem, HandlingOutlier data as missing values by imputation methods: application of machine learning algorithms, *Turk. J. Comput. Math. Educ.*, 2022, **13**(1), 273–286.

52 R. Garcia-Carretero, R. Holgado-Cuadrado and Ó. Barquero-Pérez, Assessment of classification models and relevant features on nonalcoholic steatohepatitis using random forest, *Entropy*, 2021, **23**(6), 763.

53 I. C. Suherman and R. Sarno Implementation of random forest regression for COCOMO II effort estimation. In2020 international seminar on application for technology of information and communication (iSemantic) 2020 Sep 19 (pp. 476–481). IEEE.

54 S. Yilmazer and S. Kocaman, A mass appraisal assessment study using machine learning based on multiple regression and random forest, *Land use policy*, 2020, **99**, 104889.

55 M. R. Segal Machine learning benchmarks and random forest regression.

56 M. Abbaszadeh, S. Soltani-Mohammadi and A. N. Ahmed, Optimization of support vector machine parameters in modeling of Iju deposit mineralization and alteration zones using particle swarm optimization algorithm and grid search method, *Comput. Geosci.*, 2022, **165**, 105140.

57 M. A. Abbas, W. J. Al-Mudhafar and D. A. Wood, Improving permeability prediction in carbonate reservoirs through gradient boosting hyperparameter tuning, *Earth Sci. Inform.*, 2023, **16**(4), 3417–3432.

58 K. Sandunil, Z. Bennour, H. Ben Mahmud and A. Giwelli Effects of Tuning Hyperparameters in Random Forest Regression on Reservoir's Porosity Prediction. Case Study: Volve Oil Field, North Sea. InARMA US Rock Mechanics/Geomechanics Symposium 2023 Jun 25 (pp. ARMA-2023). ARMA.

59 W. J. Al-Mudhafar Incorporation of bootstrapping and cross-validation for efficient multivariate facies and petro-physical modeling. InSPE Rocky Mountain Petroleum Technology Conference/Low-Permeability Reservoirs Symposium 2016 May 5 (pp. SPE-180277). SPE.

60 M. Rahimi and M. A. Riahi, Reservoir facies classification based on random forest and geostatistics methods in an offshore oilfield, *J. Appl. Geophys.*, 2022, **201**, 104640.

61 A. A. Mahmoud, S. Elkatatny, W. Chen and A. Abdulraheem, Estimation of oil recovery factor for water drive sandy reservoirs through applications of artificial intelligence, *Energies*, 2019, **12**(19), 3671.

62 H. Al Khalifah, P. W. Glover and P. Lorinczi, Permeability prediction and diagenesis in tight carbonates using machine learning techniques, *Mar. Pet. Geol.*, 2020, **112**, 104096.

63 W. M. Ridwan, M. Sapitang, A. Aziz, K. F. Kushiar, A. N. Ahmed and A. El-Shafie, Rainfall forecasting model using machine learning methods: Case study Terengganu, Malaysia, *Ain Shams Eng. J.*, 2021, **12**(2), 1651–1663.

64 H. Wang, Z. Lei, X. Zhang, B. Zhou and J. Peng, Machine learning basics, *Deep Learning*, 2016, 98–164.

65 P. Mehta, M. Bukov, C. H. Wang, A. G. Day, C. Richardson, C. K. Fisher and D. J. Schwab, A high-bias, low-variance introduction to machine learning for physicists, *Phys. Rep.*, 2019, **810**, 1–24.